Buckling of imperfect laminated cylinders under hydrostatic pressure

Tanguy Messager

Buckling of imperfect laminated cylinders under hydrostatic pressure

Tanguy Messager

Laboratoire d'Etudes des Structures, école HEI, 13 rue de Toul, 59046 Lille, France

The objective of this paper is to investigate numerically the influence of the winding-induced geometrical imperfection on to the elastic buckling load of submersible composite hulls. A linear Sanders-type buckling model of laminated cross-ply cylinders is developed. The imperfection is modeled by an axisymmetric thickness default of each composite ply by analogy to the real laminate ply imperfections. The effects of these defaults are taken into account by correcting the laminated stiffness coefficients. Numerical examples have been performed analyzing three types of stacking sequences for thin carbon/epoxy cylinders. For each case, the geometrical imperfections induce significant buckling load reductions. The results of the proposed approach appear to be in good agreement with standard FEM code calculus.

Keywords: Laminated cylinders; External pressure; Buckling; Imperfections

1. Introduction

The use of composite materials in the fabrication of submersible devices allows low weight to displacement ratios [1,2]. Various industrial applications concerning remotely operated vehicles and autonomous underwater vehicles have been investigated in recent papers [3–7]. For such structures, the hulls are generally realized using multilayered, cross-ply, composite cylinders obtained following the filament winding process [5,8] and closed with metallic plates at their ends [7]. Previous studies have shown numerically [2,7] and experimentally [4] that such vessels are subjected to elastic buckling phenomenon due to the external hydrostatic pressure. Thus, the limit of stability is the major design criteria of submersible cylindrical hulls. As shown in [1,9], various works have focused on the development of approaches based on analytical formulations allowing the designers to obtain fast and reliable buckling load predictions.

It is assumed that initial geometric imperfections are the main source of buckling load reductions for both isotropic [9,10] or composite [6,11] cylinders under hydrostatic pressure. These geometric defaults lead to considerable discrepancies (exceeding sometimes more than 50%) between experimental results and perfect cylinder model predictions [12,13]. For several years, many authors have studied and developed analytical models of imperfect laminated cylinders subjected to buckling. Various simple [11] or combined [13] load cases (like axial compression, lateral pressure, torsion, etc.) have been investigated in these works. These analytical models were taking into account [11] or not [14] the transverse shear effects.

The formulations of the shell models in all referenced studies have been based on a main feature which is an extension of previous analysis concerning the buckling of isotropic imperfect cylinders [9,14,15]: the geometrical imperfections is assumed to be generated by an axisymmetric modal deflection of the mean-surface of the laminated cylinder. However, as mentioned in [4], the global geometrical imperfection of a composite cylinder, realized on a mandrel following the filament winding process, appears as thickness variations. This global thickness default is due to the fact that each cross-ply of a laminated cylinder possess an axisymmetric thickness waviness due to fiber crossings during the fabrication process [5,8]. The influence of the winding-induced ply thickness imperfections, leading to a global geometrical default of the shell, is generally disregarded.

The objective of this paper is to investigate numerically the influence of the winding-induced thickness imperfections on to the elastic buckling load of laminated cylinders. A specific formulation of an analytical Sanders-type model for the buckling of imperfect laminated cylinders under external pressure is developed. The global thickness imperfection of the cylinder is assumed to be generated by the composite ply wavinesses

[5,8]. Each of these ply defaults is modeled by an axisymmetric thickness waviness by analogy to their real shapes. The effects of these ply imperfections are introduced in the problem by correcting the stiffness coefficients of the laminate. In this first approach, the basic strain–displacement and equilibrium relations are of the linear form [16]. The final expression of the eigenvalue problem of buckling is obtained using Galerkin's method. Numerical tests and comparisons with Samcef standard FEM code results are performed for three types of stacking sequences of imperfect, laminated, carbon/epoxy cylinders.

2. Theoretical analysis

This section details the analytical analysis of the elastic buckling of geometrically imperfect, composite, cross-ply, laminated cylinders. The developed analytical model is based on the Sanders-type relations [9]. This shell theory is related to the mean-surface of the cylinder and neglects the transverse shear effects. The linear buckling analysis presented below is based on the method of adjacent equilibrium [13]. The imperfection model is detailed in Section 2.2.

2.1. Basic relations of the Sanders-type model

The geometry of the shell is characterized by its length L, its mean-radius R and the wall-thickness h. As shown in Fig. 1, the x, y and z coordinates and the corresponding u, v and w displacements are measured in the axial, circumferential and radial directions, respectively, with respect to the cylindrical mean-surface [14]. Due to the filament winding fabrication process [8], each kth composite layer is assumed to be orthotropic and cross-ply, i.e., made up of equal amounts of fibers evenly distributed through its thickness in the $+\theta_k$ and $-\theta_k$ directions with respect to the cylinder axis.

The linear strain–displacement relations [9] are expressed in the following form:

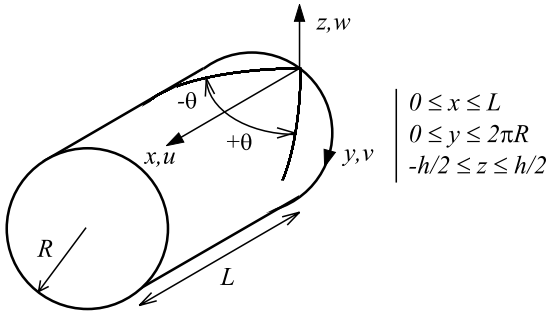

Fig. 1. Geometry of the cylindrical shell.

$$\begin{Bmatrix} \varepsilon_{xx} \\ \varepsilon_{yy} \\ 2\varepsilon_{xy} \end{Bmatrix} = \left([\Gamma_\varepsilon] + z[\Gamma_\chi]\right) \begin{Bmatrix} u \\ v \\ w \end{Bmatrix} = \left(\begin{bmatrix} \frac{\partial}{\partial x} & 0 & 0 \\ 0 & \frac{\partial}{\partial y} & \frac{1}{R} \\ \frac{\partial}{\partial y} & \frac{\partial}{\partial x} & 0 \end{bmatrix} + z \begin{bmatrix} 0 & 0 & -\frac{\partial^2}{\partial x^2} \\ 0 & \frac{1}{R}\frac{\partial}{\partial y} & -\frac{\partial^2}{\partial y^2} \\ 0 & \frac{2}{R}\frac{\partial}{\partial x} & -2\frac{\partial^2}{\partial x \partial y} \end{bmatrix} \right) \begin{Bmatrix} u \\ v \\ w \end{Bmatrix}. \quad (1)$$

The elastic orthotropic constitutive law for the kth composite ply is given by

$$\begin{Bmatrix} \sigma_{xx}^{(k)} \\ \sigma_{yy}^{(k)} \\ \sigma_{xy}^{(k)} \end{Bmatrix} = \begin{bmatrix} Q_{11}^{(k)} & Q_{12}^{(k)} & Q_{16}^{(k)} \\ Q_{12}^{(k)} & Q_{22}^{(k)} & Q_{26}^{(k)} \\ Q_{16}^{(k)} & Q_{66}^{(k)} & Q_{66}^{(k)} \end{bmatrix} \begin{Bmatrix} \varepsilon_{xx}^{(k)} \\ \varepsilon_{yy}^{(k)} \\ 2\varepsilon_{xy}^{(k)} \end{Bmatrix}, \quad (2)$$

where the $Q_{ij}^{(k)}$ are the corresponding orthotropic, reduced, constitutive coefficients detailed in [14]. Considering that each composite ply is cross-ply, the following terms characterizing the coupling between shearing and extensional strain are equal to zero [9]

$$Q_{16}^{(k)} = Q_{26}^{(k)} = 0. \quad (3)$$

The force and moment resultants [15] related to the mean-surface are expressed as follows:

$$\{N\} = \begin{Bmatrix} N_{xx} \\ N_{yy} \\ N_{xy} \end{Bmatrix} = \int_{h/2}^{h/2} \begin{Bmatrix} \sigma_{xx} \\ \sigma_{yy} \\ \sigma_{xy} \end{Bmatrix} \mathrm{d}z \quad \text{and}$$

$$\{M\} = \begin{Bmatrix} M_{xx} \\ M_{yy} \\ M_{xy} \end{Bmatrix} = \int_{h/2}^{h/2} \begin{Bmatrix} \sigma_{xx} \\ \sigma_{yy} \\ \sigma_{xy} \end{Bmatrix} z \,\mathrm{d}z. \quad (4)$$

The three governing equations of equilibrium are defined by

$$[\Gamma_{\mathrm{eq}}] \begin{Bmatrix} \{N\} \\ \{M\} \\ \{F\} \end{Bmatrix} = \begin{bmatrix} \frac{\partial}{\partial x} & 0 & \frac{\partial}{\partial y} & 0 & 0 & 0 & 0 & 0 \\ 0 & \frac{\partial}{\partial y} & \frac{\partial}{\partial x} & 0 & \frac{1}{R}\frac{\partial}{\partial y} & \frac{1}{R}\frac{\partial}{\partial x} & 0 & \frac{1}{R} \\ 0 & -\frac{1}{R} & 0 & \frac{\partial^2}{\partial x^2} & \frac{\partial^2}{\partial x^2} & 2\frac{\partial^2}{\partial x \partial y} & \frac{\partial}{\partial x} & \frac{\partial}{\partial y} \end{bmatrix} \begin{Bmatrix} \{N\} \\ \{M\} \\ \{F\} \end{Bmatrix} = 0, \quad (5)$$

where $\{F\}$ introduced the resulting components of the hydrostatic external pressure loading P related to the mean-surface [9]. These components are defined as follows

$$\{F\} = \begin{Bmatrix} F_x \\ F_y \end{Bmatrix} = P[\Gamma_F] \begin{Bmatrix} u \\ v \\ w \end{Bmatrix} = P \begin{bmatrix} 0 & 0 & -\frac{R}{2}\frac{\partial}{\partial x} \\ 0 & 1 & -R\frac{\partial}{\partial y} \end{bmatrix} \begin{Bmatrix} u \\ v \\ w \end{Bmatrix}. \quad (6)$$

According to previous modeling studies [7,12], the cylinders are assumed to be simply supported at their ends. Thus, the chosen displacement mean-surface field satisfying these boundary conditions is [15]

$$\begin{Bmatrix} u \\ v \\ w \end{Bmatrix} = [\phi]\{a\} = \begin{bmatrix} \phi_u & 0 & 0 \\ 0 & \phi_v & 0 \\ 0 & 0 & \phi_w \end{bmatrix} \begin{Bmatrix} a_u \\ a_v \\ a_w \end{Bmatrix}, \tag{7}$$

where $\{a\}$ is the eigen-displacement vector of the buckling problem. The displacement approximation functions are expressed in the following forms:

$$\begin{cases} \phi_u = \cos(\bar{m}x)\cos(\bar{n}y) \\ \phi_v = \sin(\bar{m}x)\sin(\bar{n}y) \\ \phi_w = \sin(\bar{m}x)\cos(\bar{n}y) \end{cases} \quad \text{with} \quad \begin{cases} \bar{m} = m\pi/L, \\ \bar{n} = n/R, \end{cases} \tag{8}$$

where m and n are the numbers of longitudinal and circumferential half waves respectively, characterizing the buckling mode as shown in Fig. 2.

2.2. Geometrical imperfection model

Each ply of a cylinder obtained following the filament winding process is subjected to longitudinal axisymmetric wavinesses due to the fiber crossings that generate a global geometrical thickness imperfection of the shell [5,8]. The maximum amplitude value $\tilde{a}$ of each cross-ply thickness axisymmetric default is then defined as

$$\tilde{a} = \quad \overline{2}\tilde{\mu}/q = \tilde{h}/q, \tag{9}$$

where $\tilde{\mu}$ is the root-mean-square value of the geometrical imperfection profiles [9] (measured on the external surfaces of the cylinder), $\tilde{h}$ the equivalent maximum amplitude of these global imperfection of the cylinder [9,13] and q is the total number of cross-ply. By analogy to their real shapes, each of the ply defaults is modeled by an axisymmetric thickness waviness expressed as follows:

$$\begin{aligned} \tilde{z}_k &= z_k + \tilde{w}, \\ \tilde{z}_{k-1} &= z_{k-1} - \tilde{w}. \end{aligned} \tag{10}$$

The imperfection component $\tilde{w}$ is given by

$$\tilde{w} = \tilde{a}\sin(\tilde{m}\pi x/L), \tag{11}$$

where $\tilde{m}$ is the number of the longitudinal half waves of the ply thickness imperfection. The ply thickness imperfection model is illustrated in Fig. 3.

The effects of these ply imperfections are taken into account in the stiffness coefficients of the laminate. Replacing z in Eq. (4) by the $\tilde{z}$ form defined in the previous

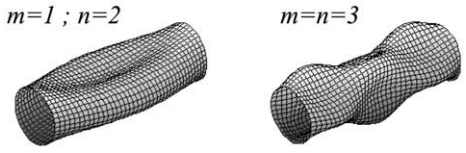

Fig. 2. Examples of buckling modes.

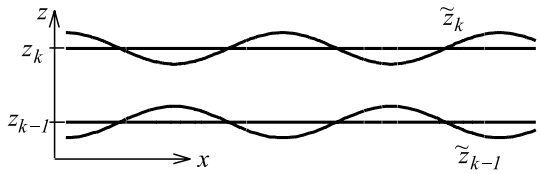

Fig. 3. Imperfect thickness model for a kth ply.

Eqs. (10) and (11), we obtained the following expressions for the stress and moment resultants:

$$\begin{Bmatrix} \{N\} \\ \{M\} \end{Bmatrix} = \begin{bmatrix} [\tilde{A}] & [\tilde{B}] \\ [\tilde{B}] & [\tilde{D}] \end{bmatrix} \begin{Bmatrix} [\Gamma_\varepsilon] \\ [\Gamma_\chi] \end{Bmatrix} \begin{Bmatrix} u \\ v \\ w \end{Bmatrix}. \tag{12}$$

The corrected stiffness coefficients are given by

$$\begin{cases} \tilde{A}_{ij} = A_{ij}\left(1 - \frac{2\tilde{w}}{h}\right) \\ \tilde{B}_{ij} = B_{ij} - A'_{ij}\tilde{w} \\ \tilde{D}_{ij} = D_{ij} - B'_{ij}\tilde{w} + A'_{ij}\left(\tilde{w}^2 - \frac{2\tilde{w}^3}{3h}\right) \end{cases} \quad (i,j = 1,2,6). \tag{13}$$

The A_{ij}, B_{ij} and D_{ij} terms are the classical laminate stiffness coefficients of membrane, coupling and bending, respectively [15]

$$\begin{aligned} A_{ij} &= \sum_{k=1}^{q} Q_{ij}^{(k)} h_k, \\ B_{ij} &= \frac{1}{2}\sum_{k=1}^{q} Q_{ij}^{(k)}\left(z_k^2 - z_{k-1}^2\right), \\ D_{ij} &= \frac{1}{3}\sum_{k=1}^{q} Q_{ij}^{(k)}\left(z_k^3 - z_{k-1}^3\right). \end{aligned} \tag{14}$$

The additional stiffness terms, taking into account the geometrical axisymmetric ply imperfections are defined as follows:

$$\begin{aligned} A'_{ij} &= \sum_{k=1}^{q} Q_{ij}^{(k)}(z_k + z_{k+1}), \\ B'_{ij} &= \sum_{k=1}^{q} Q_{ij}^{(k)}\left(z_k^2 + z_{k-1}^2\right). \end{aligned} \tag{15}$$

2.3. Final form of the eigen-problem

Substituting Eqs. (1), (6) and (12) in Eq. (5), the equilibrium can be expressed as follows:

$$[\Gamma]\begin{Bmatrix} u \\ v \\ w \end{Bmatrix} = [\Gamma_{\text{eq}}]\left\{ \begin{bmatrix} [\tilde{A}] & [\tilde{B}] \\ [\tilde{B}] & [\tilde{D}] \\ & P[\Gamma_F] \end{bmatrix} \begin{Bmatrix} [\Gamma_\varepsilon] \\ [\Gamma_\chi] \end{Bmatrix} \right\} \begin{Bmatrix} u \\ v \\ w \end{Bmatrix} = 0. \tag{16}$$

Considering the field of buckling displacements defined in Eqs. (7) and (8), the Galerkin's variational formulation of the equilibrium [14] is given by

$$\int_0^L \int_0^{2\pi R} [\phi][\Gamma][\phi]\,\mathrm{d}x\,\mathrm{d}y\{a\} = 0. \tag{17}$$

As for numerous previous modeling studies [9,13,14], the Galerkin's procedure requires an additional assumption to obtain a non-zero problem. For the presented model, the $\tilde{m}$ value is required to be

$$\tilde{m} = 2m. \tag{18}$$

The integration of Eq. (16) then leads to the eigenvalue problem of the simple form

$$[K] + P[L] = 0. \tag{19}$$

The corresponding K_{ij} and L_{ij} $(i,j = 1,2,3)$ terms are detailed in Appendix A. The critical external pressure P_{cr} corresponds to the lowest P value satisfying to Eq. (19).

3. Numerical examples

This section presents numerical results for the buckling of thin-walled carbon/epoxy cylinders. Three type of stacking sequence patterns have been considered. The buckling pressure are investigated using the Sanders-type model detailed in the previous section. Moreover, FEM calculus using SAMCEF code were carried for comparison: the cylinders were modeled using hybrid, composite laminated, shell elements. The rigid end-closures were modeled by rigid body elements leading to simply supported boundary conditions [7,10]. As for the most part of the standard FEM codes, SAMCEF takes into account the global geometrical imperfection influence by introducing a modal deviation in the coordinate values of the nodes. The buckling pressures were obtained by performing linear analysis of stability.

The geometry of the considered cylinders is determined by (in mm): $R = 75$; $L = 450$; $h = 6$. These thin-walled cylinders are composed of 10 composite cross-plies of equal thicknesses. The constituting material is a carbon fiber reinforced epoxy resin. The orthotropic in-plane mechanical characteristics are (modulus in GPa): $E_1 = 156$; $E_2 = 9.65$; $G_{12} = 5.47$; $\nu_{12} = 0.27$ (where subscripts 1 and 2 denote the longitudinal and perpendicular directions of the fibers, respectively). Three following types of stacking sequences are studied (angles in degrees notice from the inner to the outer surface of the tube)

$$[\theta_{10}]; \quad [(90/\theta)_5]; \quad [90_3/\theta_4/90_3].$$

Fig. 4 presents the evolution of the critical external hydrostatic pressure P_{cr} as a function of the cross-ply angle value θ. As shown, the discrepancies between the analytical and the FEM results appear to be generally less than 5% and less than 10% for the worst cases. The global tendencies of the buckling pressure evolutions calculated both analytically and by FEM model are equivalent. The corresponding buckling modes (generally $m = 1$ and $n = 2$, as presented in Fig. 2) are always in good agreement.

It is worth noting that Fig. 4 shows considerable differences of buckling pressure values between the different lamination cases: the lowest value was found to be $P_{cr} \approx 5$ MPa and corresponds to the $[0_{10}]$ stacking sequence. The $[90_3/20_4/90_3]$ lamination then leads to $P_{cr} \approx 30$ MPa. Thus, as shown numerically and experimentally in a previous work detailed in [17,18], the choice of an appropriated stacking sequence allows to increase notably the limit of stability.

For the study of the imperfection sensitivities, three cases of θ values were investigated for the previous three stacking sequences

$$\theta = \{0; 30; 60\}.$$

The $[90_{10}]$ lamination case was improved too. The measure of the buckling pressure reduction due to imperfections is realized both for the FEM and the

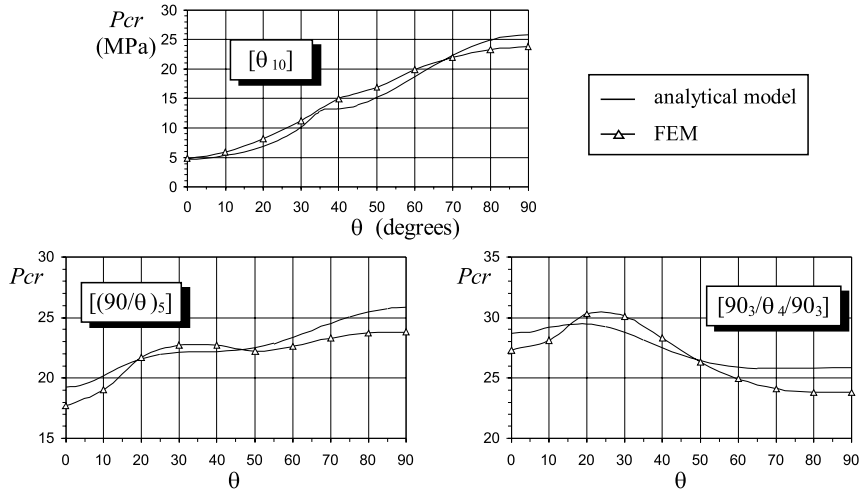

Fig. 4. Critical pressure evolutions for perfect cylinders.

analytical models using the critical pressure reduction factor δ defined as follows:

$$\delta = Pcr(\tilde{h})/Pcr(\tilde{h}=0). \tag{20}$$

Fig. 5 presents the analytical and FEM results for different values of the equivalent imperfection maximum amplitude $\tilde{h}$. It is worth to note that each buckling pressure calculus requires less than 1 s CPU time (on a UltraSparc Sun workstation) for the analytical model. Each FEM calculus needs about 5 min CPU time.

For each stacking sequence studied, the δ evolution obtained analytically appears to be quasi-linear. However, the FEM and analytical δ evolutions are closer. The differences between the δ values obtained analytically and by FEM models are always less than 10%. Moreover, as shown in previous studies [6,11,14], the stacking sequences appear to influence the δ values and evolutions. This influence is apparent both for the FEM and the analytical results.

The developed analytical model allows quite reliable estimations of the buckling pressure reductions due to geometrical imperfections. In the problem under consideration, the proposed approach can appropriately replace complex FEM models and calculus requiring substantial CPU time. Thus, the developed analytical model can be a practical and fast way for designers to estimate the buckling external pressure of imperfect laminated cylinders.

4. Conclusion

An analytical linear model for the buckling of composite laminated cylinders under external hydrostatic pressure was developed in order to take into account the influence of winding-induced geometrical defaults. By analogy to the real thickness section of laminated cylinders, the geometrical imperfections are assumed to be generated by cross-ply defaults modeled as axisymmetric imperfections.

Numerical tests were performed for different lamination cases of thin-walled, imperfect, carbon/epoxy cylinders. Calculus were carried out using both the analytical model and a FEM code. The geometrical imperfections lead to drastic buckling load decrease. For the imperfect cylinders, the buckling pressure reductions obtained from the analytical model were in good agreement with FEM results. The developed analytical

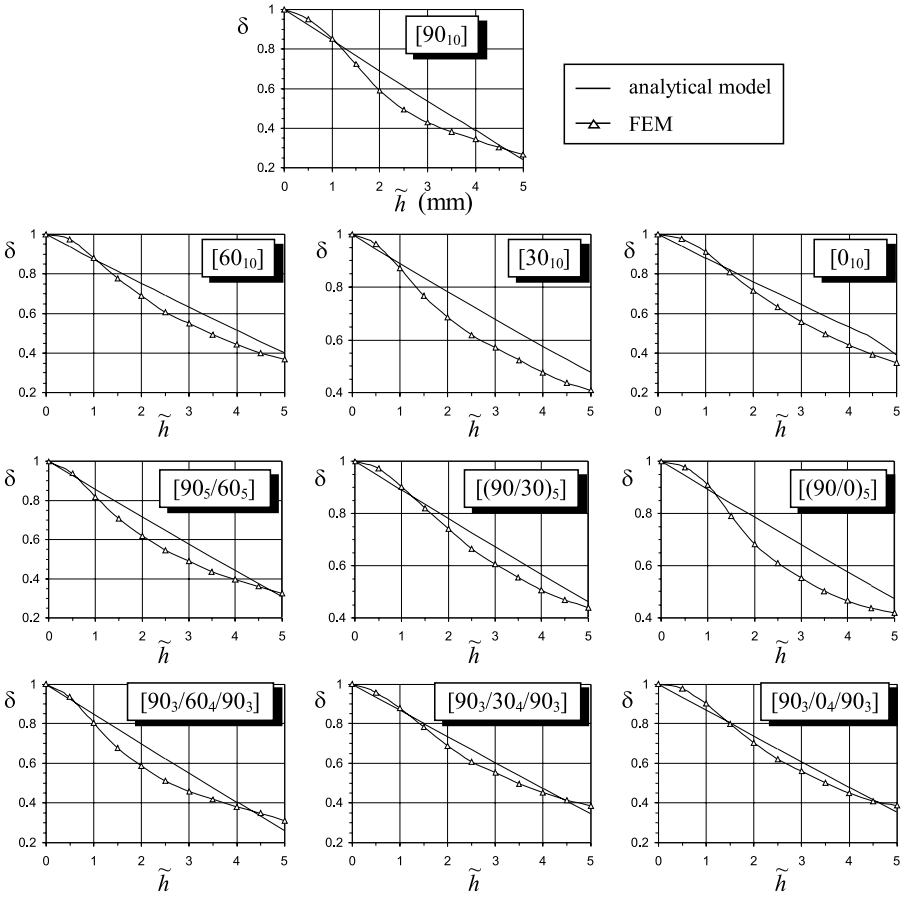

Fig. 5. Critical pressure reductions for imperfect cylinders.

model appears to be a practical method to estimate the buckling pressure of imperfect, laminated, submersible, cylindrical hulls.

Medium-thick and thick-walled composite cylinders are very sensitive to the transverse shear effects [11,16]. Moreover, as mentioned by numerous authors (e.g. [9,13,15,19]), the geometrical non-linearities have a great influence in the actual shell buckling load levels. In order to obtain more realistic and accurate evaluations of cylinder stability limits, complementary studies are intended to be carried out to extend the developed geometrical imperfection model to a high-order shear deformable and non-linear cylinder theory.

Acknowledgements

The author wishes to acknowledge IFREMER (the French Research Institute for the Exploitation of the Sea – Brest Center) for its aid. Moreover, this work has been supported by the "Conseil Régional de Bretagne" and the MAS3-CT97-0091 project of the European Community MAST program. Dr. Mariusz Pyrz (University of Science and Technology of Lille) is also gratefully acknowledged for its assistance.

Appendix A

$$K_{11} = A_{11}\bar{m}^2\left(1-\frac{\tilde{a}}{h}\right) + A_{66}\bar{n}^2\left(1+\frac{\tilde{a}}{h}\right),$$

$$K_{12} = -\left[A_{12}\left(1-\frac{\tilde{a}}{h}\right) + A_{66}\left(1+\frac{\tilde{a}}{h}\right) + \frac{B_{12}+2B_{66}}{R} - \frac{\tilde{a}}{2R}\left(A'_{12}-2A'_{66}\right)\right]\bar{m}\bar{n},$$

$$K_{13} = K_{31} = \frac{A_{12}\bar{m}}{R}\left(\frac{\tilde{a}}{h}-1\right) - B_{11}\bar{m}^3 - (B_{12}+2B_{66})\bar{m}\bar{n}^2 + \frac{\tilde{a}}{2}\left[A'_{11}\bar{m}^3 + \left(A'_{12}-2A'_{66}\right)\bar{m}\bar{n}^2\right],$$

$$K_{21} = -\left[A_{12}\left(1-\frac{\tilde{a}}{h}\right) + A_{66}\left(1+\frac{\tilde{a}}{h}\right) + \frac{B_{12}+B_{66}}{R} - \frac{\tilde{a}}{2R}\left(A'_{12}-A'_{66}\right)\right]\bar{m}\bar{n},$$

$$K_{22} = A_{22}\left(1-\frac{\tilde{a}}{h}\right)\bar{n}^2 + A_{66}\left(1+\frac{\tilde{a}}{h}\right)\bar{m}^2 + \frac{1}{R}\left(2B_{22}\bar{n}^2 + 3B_{66}\bar{m}^2 + \frac{D_{22}\bar{n}^2+2D_{66}\bar{m}^2}{R}\right) - \frac{\tilde{a}}{2R}\left(2A'_{22}\bar{n}^2 - 3A'_{66}\bar{m}^2 + \frac{B'_{22}\bar{n}^2-2B'_{66}\bar{m}^2}{R}\right) + \frac{A_{22}\bar{n}^2}{2R^2}\left(\tilde{a}^2-\frac{3\tilde{a}^3}{2h}\right) + \frac{A_{66}\bar{m}^2}{R^2}\left(\tilde{a}^2+\frac{3\tilde{a}^3}{2h}\right),$$

$$K_{23} = \frac{A_{22}\bar{n}}{R}\left(1-\frac{\tilde{a}}{h}\right) + B_{22}\left(\bar{n}^3+\frac{\bar{n}}{R^2}\right) + (B_{12}+2B_{66})\bar{m}^2\bar{n} + \frac{D_{22}\bar{n}^3+(D_{12}+2D_{66})\bar{m}^2\bar{n}}{R} - \frac{\tilde{a}}{2}\left[A'_{22}\left(\bar{n}^3+\frac{\bar{n}}{R^2}\right) + \left(A'_{12}+2A'_{66}\right)\bar{m}^2\bar{n} + \frac{B'_{22}\bar{n}^3+\left(B'_{12}+2B'_{66}\right)\bar{m}^2\bar{n}}{R}\right] + \frac{A_{22}\bar{n}^3+A_{12}\bar{m}^2\bar{n}}{2R}\left(\tilde{a}^2-\frac{\tilde{a}^3}{2h}\right) + \frac{A_{66}\bar{m}^2\bar{n}}{2R}\left(\tilde{a}^2+\frac{\tilde{a}^3}{2h}\right),$$

$$K_{32} = \frac{A_{22}\bar{n}}{R}\left(1-\frac{\tilde{a}}{h}\right) + B_{22}\left(\bar{n}^3+\frac{\bar{n}}{R^2}\right) + (B_{12}+2B_{66})\bar{m}^2\bar{n} + \frac{D_{22}\bar{n}^3+(D_{12}+4D_{66})\bar{m}^2\bar{n}}{R} - \frac{\tilde{a}}{2}\left[A'_{22}\left(\bar{n}^3+\frac{\bar{n}}{R^2}\right) + \left(A'_{12}+2A'_{66}\right)\bar{m}^2\bar{n} + \frac{B'_{22}\bar{n}^3+\left(B'_{12}+4B'_{66}\right)\bar{m}^2\bar{n}}{R}\right] + \frac{A_{22}\bar{n}^3+A_{12}\bar{m}^2\bar{n}}{2R}\left(\tilde{a}^2-\frac{\tilde{a}^3}{2h}\right) + \frac{A_{66}\bar{m}^2\bar{n}}{2R}\left(\tilde{a}^2+\frac{\tilde{a}^3}{2h}\right),$$

$$K_{33} = \frac{A_{22}}{R^2}\left(1-\frac{\tilde{a}}{h}\right) + \frac{2}{R}\left(B_{12}\bar{m}^2+B_{22}\bar{n}^2\right) + D_{11}\bar{m}^4 + D_{22}\bar{n}^4 + 2(D_{12}+2D_{66})\bar{m}^2\bar{n}^2 - \frac{\tilde{a}}{2}\left[\frac{2}{R}\left(A'_{12}\bar{m}^2+A'_{22}\bar{n}^2\right) + B'_{11}\bar{m}^4 + B'_{22}\bar{n}^4 + 2\left(B'_{12}-2B'_{66}\right)\bar{m}^2\bar{n}^2\right] + \frac{A_{11}\bar{m}^4+A_{22}\bar{n}^4+2A_{12}\bar{m}^2\bar{n}^2}{2}\left(\tilde{a}^2-\frac{\tilde{a}^3}{2h}\right) + \frac{A_{66}\bar{m}^2\bar{n}^2}{2}\left(\tilde{a}^2+\frac{\tilde{a}^3}{2h}\right),$$

$$L_{11} = L_{12} = L_{13} = L_{21} = L_{31} = 0; \quad L_{22} = 1/R;$$

$$L_{23} = L_{32} = \bar{n}; \quad L_{33} = \left(\frac{\bar{m}^2}{2}+\bar{n}^2\right)R.$$

References

[1] Vinson JR. The behavior of shells composed of isotropic and composite materials. Dordrecht: Kluwer Academic Publishers; 1992.

[2] Graham D. Composite pressure hulls for deep ocean submersibles. Compos Struct 1995;32:331–43.

[3] Davies P, et al. Matériaux composites pour véhicule sous-marin 6000 métres. In: Proceedings of the 10eme Journées Nationales Composites (JNC10), 1996 29–31 October; Paris. p. 525–35.

[4] Davies P, Chauchot P. Composites for marine applications – part 2: underwater structures. In: Mechanics of composite materials and structures. Dordrecht: Kluwer Academic Publishers; 1999. p. 249–60.

[5] Dvorak GJ, Prochazka P. Thick-walled composites cylinders with optimal fiber prestress. Composites Part B 1996;27b:643–9.

[6] Sridharan S, Kasagi A. On the buckling and collapse of moderately thick composite cylinders under hydrostatic pressure. Composites Part B 1997;28b:583–96.

[7] Papazoglou VJ, Tsouvalis NG, Zaphiratou AA. Parametric study of small scale cylinders under hydrostatic load: flat rigid end closures. MAST III project MAS3-CT97-0091, report no. STL-073-F-98. National Technical University of Athens; 1998.

[8] Rousseau J, Perreux D, Verdiere N. Motifs d'enroulement et endommagement dans les tubes composites verre/époxy (Filament winding and damage in glass/epoxy composite pipes). Mécanique Industrielle et Matériaux 1997;5(3):155–8.

[9] Barbe J. Structures coques – équations générales et stabilité. Toulouse, France: Ensae; 1983.

[10] Guggenberger W. Buckling and postbuckling of imperfect cylindrical shells under external pressure. Thin-Walled Struct 1995;23:351–66.

[11] Tabiei A, Simitses G. Imperfections sensitivity of shear deformable moderately thick laminated cylindrical shells. Comput Struct 1997;62(1):165–74.

[12] Ouellette P, Hoa SV, Sankar TS. Buckling of composite cylinders under external pressure. Polym Compos 1986;7(5):363–74.

[13] Sun G, Hansen JS. Optimal design of laminated composite circular–cylindrical shells subjected to combined loads. J Appl Mech 1988;55:136–42.

[14] Tennyson RC, Chan KH, Muggeridge DB. The effect of axisymetric shape imperfections on the buckling of laminated anisotropic circular cylinders. CASI Trans 1971;4(2):131–9.

[15] Soldatos KP. Nonlinear analysis of transverse shear deformable laminated composite cylindrical shells. J Pressure Vessel Technol 1992;114:105–14.

[16] Simitses GJ. Buckling of moderately thick laminated cylindrical shells: a review. Composites Part B 1996;27b:581–7.

[17] Messager T, Pyrz M, Chauchot P. Optimized laminations for submarine composite hulls. Eur J Finite Elements 2000; 9(1-2-3):199–215.

[18] Messager T, Chauchot P, Gineste B, Bigourdan B. Optimisation d'enceintes sous-marines composites – validation expérimentale (Optimization of composite submarine hulls – experimental validation). In: 5eme Colloque National en Calcul des Structures (Giens'2001), 2001 15–18 May; Giens, France (accepted).

[19] Greenberg JB, Stavsky Y. Buckling of composite orthotropic cylindrical shells under non-uniform axial loads. Compos Struct 1995;30:399–406.